Supporting Information

Gong et al. 10.1073/pnas.1716620115

Initial Spreading Speed Determines the Final Spreading Area

At the beginning of cell spreading, myosins pull the actin filaments toward the cell center with a characteristic force f_m, while the engaged clutches resist the retrograde actin flow by the adhesion force f_{FA}. In this stage, the actin polymerization velocity V_p is only countered by the retrograde flow speed V_r, and hence the initial spreading speed is simply $V_s = V_p - V_r$. As cell spreading progresses, the deformed membrane and cytoskeleton will also start to resist the further growth of the F-actin bundle, eventually leading to a steady-state cell spreading area (Fig. S2*A*). To connect the steady-state spreading area with the initial spreading speed, we assumed the resistance force generated by the deformed cytoskeleton and membrane is f_c. Under such circumstance, the force equilibrium becomes

$$f_{FA} = f_c + f_m. \quad \textbf{[S1]}$$

If, for simplicity, the cytoskeleton/membrane is treated as a viscoelastic material with height h (i.e., the thickness of lamellipodium), the resistance force f_c can be calculated as (1, 2)

$$f_c = h\sigma_r = h\left(k_m\epsilon_r + \eta_m\frac{d\epsilon_r}{dt}\right). \quad \textbf{[S2]}$$

Here k_m and η_m are the effective stiffness and viscosity, respectively, of the cytoskeleton, and $\epsilon_r = R(t) - R_0/R_0$ is the mean radial strain in the deformed cytoskeleton with $R(t)$ being the spreading radius at time t. The incorporation of these two equations into motor clutch framework is shown in the flowchart in Fig. S2*F*. Specifically, we integrated the spreading speed to obtain the spreading radius at each time step and updated the membrane resistance force before calculating the force from the myosin motors. This process is repeated for 5,000 s with a time step of 5 ms to ensure that steady-state radius is indeed reached. By carrying out the KMC simulations, the entire spreading process (i.e., from the initial spreading to the eventual steady-state configuration) can be captured. Clearly, the fraction of bounded clutches and retrograde flow again exhibits continuous load and fail behavior (Fig. S2 *B* and *C*, *Insets*), while the spreading radius initially increases rapidly and gradually approaches a steady-state value (Fig. S2*D*). At the steady state, the retrograde flow would fully counter the polymerization speed, $V_p = V_r$, leading to zero spreading velocity (Fig. S2*C*). Clearly, larger cell spreading velocity also indicates larger cell spreading area, which is in accordance with previous study (2). More importantly, a linear relationship between the initial spreading speed and the steady-state spreading radius was observed from our simulations (Fig. S2*E*). This linear relation allows us to characterize the steady-state cell spreading radius R_{ss} (and the area πR_{ss}^2) from the initial spreading radius R_0 and steady spreading timescale τ_{ss} (i.e., $R_{ss} = R_0 + V_s \cdot \tau_{ss}$). The τ_{ss} can be calculated simply by $(R_{ss} - R_0)/V_s$, where the steady-state radius is determined from the experimentally measured area. Note that the spreading timescale τ_{ss} is fixed for the same cell type, and the real spreading time is usually much larger than the timescale τ_{ss}.

Mean-Field Analysis

One drawback of the KMC method is that thousands or even tens of thousands of independent simulations must be carried out to obtain the mean behavior of the system with statistical significance. In comparison, by applying the mean-field theory (3), we can average all clutches' behavior into one ensemble clutch with effective stiffness $k_c n_c P_b$. The parametric study and timescale analysis can be conducted in a much more efficient manner. Specifically, if we interpret P_b, x_c, and F_c as the average binding probability, displacement, and force transmitted, respectively, of any clutch, then the governing equations of the system (Eqs. **1**–**5**) can be written as

$$\frac{dP_b}{dt} = (1 - P_b)r_{on} - P_b\langle r_{off}\rangle \quad \textbf{[S3]}$$

$$(k_a + k_l)\eta\frac{dx_s}{dt} + k_a k_l x_s = k_a F_s + \eta\frac{dF_s}{dt} \quad \textbf{[S4]}$$

$$F_s = k_c n_c P_b (x_c - x_s) \quad \textbf{[S5]}$$

$$\frac{dx_c}{dt} = v_u \cdot \left(1 - \frac{F_s}{n_m F_m}\right). \quad \textbf{[S6]}$$

The ensemble clutch is assumed to remain bounded during its lifetime, and hence its filament end moves with the retrograde flow velocity V_f,

$$\frac{dx_c}{dt} = V_f. \quad \textbf{[S7]}$$

The mean disassociation rate is calculated as $\langle r_{off}\rangle = r_{off}^0 \cdot \exp(F_c/F_b)$, where the characteristic breakage force F_b was chosen as 1.3 pN. To account for the increased integrin density observed on stiff substrate, the clutch reinforcement mechanism (4) was implemented. Here, instead of using integrins added for each reinforcement event (4) that is affected by the simulation time step interval and number, we assume that the reinforcement extent is linearly related to the clutch force. Basically, the integrin density is assumed to undergo a portion increase, by the amount $\alpha(F_a - F_{cr})$, once the average FA force F_a (during each lifetime cycle) is above a threshold level F_{cr}. Here α, a parameter that represents sensitivity of the binding rate with increased clutch force, was set as 0.2/pN (see *General Model Parameters* for parameter choice). In this case, the clutch binding rate becomes $r_{on} = r_{on}^0(1 + \alpha(F_a - F_{cr}))$, which will then be updated in the next FA lifetime cycle. At least 10 life cycles are simulated to get the average behavior for nondivergent cases.

The spreading velocity is given by $V_s = V_p - V_f$ where V_p is the polymerization speed of actin bundle (5). It must be pointed out that, instead of using a fixed simulation time to calculate the cell spreading velocity, which is problematic for FAs with extremely long lifetimes, we evaluated the mean spreading velocity over one formation–breakage cycle in this study. Specifically, a simple average of V_f in every time step was recorded in KMC simulation to obtain the mean retrograde velocity. On the other hand, the total clutch displacement x_c in the time t_{total} was calculated in the mean-field approach, i.e., by solving the ODEs described in Eqs. **S2**–**S7**, from which the average retrograde flow speed can be estimated as (Fig. 1*D*)

$$V_f = \frac{x_c}{t_{\text{total}}}. \quad \textbf{[S8]}$$

The values of all of the parameters adopted in the KMC simulation and ODE solution are listed in Table S1. Typical results from both approaches are given in Fig. 1 *B*–*D*, which show good

agreement with each other. Clutches quickly become engaged at the beginning and then gradually break with increasing load.

Binding Timescale and the Characteristic Lifetime Dictate the Behavior of FAs

Similar to the case of a pure elastic substrate (6), we proceeded by examining the behavior of a cluster of clutches in a single formation–breakage cycle as well as how such a response is influenced by different parameters (Fig. S1 *C* and *D*). At the initial stage ($t < t_{\text{bind}}$), the tension sustained by each engaged clutch is very small, leading to a negligible dissociation rate. Hence, the clutches would form bonds very quickly, with a characteristic binding timescale $\tau_b = 1/r_{on}$. For a stable FA formed in the load and fail regime, the binding time can be estimated (by assuming most clutches become engaged) as $t_{\text{bind}} \approx \ln(N_c)/r_{on}$ (3). As motors keep pulling the actin bundle toward cell center, the clutches would sustain higher loads and start to break, reflected by a gradual drop in the fractional probability P_b after the initial binding stage (Fig. S1). Finally, all clutches become broken at $t = t_{\text{life}}$ (often referred to as the lifetime of FA cluster), which effectively completes the formation–breakage cycle. Note that t_{life} can be approximately estimated as $t_{\text{life}} \approx F_{s,\,\max}/v_u k_s$, i.e., the time needed for the substrate force F_s to reach its maximum at substrate deformation force rate, $v_u k_s$. Here, k_s represents the effective stiffness of the substrate. Considering the limiting scenario where FAs exist for a long time, the maximum substrate force ($F_{s,\max}$) in this case is simply the total myosin pulling force $F_m N_m$, while k_s should be interpreted as the long-term stiffness of the substrate, leading to a characteristic lifetime scale $\tau_l = F_m N_m / v_u k_l$.

Basically, depending on values of two timescales τ_b and τ_l, which approximately describe the binding time ($t_{\text{bind}} \propto \tau_b$) and lifetime ($t_{\text{life}} \propto \tau_l$) of the FA, the clutch and cell spreading behave totally differently. Specifically, if τ_l is larger than τ_b (Fig. S1*C* black curve), a large number of clutches will remain engaged before total rupture occurs, a scenario referred to as the load and fail. However, when the substrate becomes stiffer (corresponding to $\tau_l < 1/r_{on}^0$), the clutch reinforcement begins to take effect, while the timescale analysis before does not apply. The gradual increasing integrin density due to reinforcement mechanism elevates binding rate, which further extends FAs lifetime greatly (Fig. S1 *C* and *D*). These long stable FAs could offer large resistance force consistently to counter the retrograde flow, thus promoting the cell spreading.

As a comparison, we also discuss the case without clutch reinforcement. Similarly, when $\tau_l > \tau_b$, since the average clutch force has reached threshold value, the reinforcement will not have an effect. The clutches would perform the same load and fail behaviors (Fig. S1*B*, regime I). If $\tau_l < \tau_b$, then no stable clutches or adhesion can be formed. Instead, the FA cluster goes through rapid binding and breakage (as shown by the green line in Fig. S3 *A* and *B*), with its lifetime typically less than 1 s. Under such circumstances, labeled as the frictional slippage regime, the substrate displacement is almost negligible, while the retrograde flow velocity is essentially the polymerization speed, resulting in stalling of cell spreading. In this case, an optimum ECM stiffness leading to maximized spreading speed can be obtained in this transitional regime when the cluster binding time equals its lifetime (3). Hence, a medium substrate stiffness (~1 pN/nm) will promote cell spreading, a conclusion that is (not surprisingly) also obtained from our results under low ECM viscosity conditions (Fig. S3*C*).

Extracting Substrate Parameters from Relaxation Test

The substrate stiffness is proportional to the elastic modulus, and their conversion requires a length scale. Based on the Boussinesq Green's function approach (7), the spring constant of substrate with contact radius R can be written as

$$k_c = \frac{4}{7}\frac{\pi R E}{(1+\nu)(1-0.86\,\nu)} \approx 2\,RE. \qquad \textbf{[S9]}$$

Here we assumed the Poisson's ratio $\nu = 0.5$, and, since experiments have shown that the length of FAs is typically on the order of a micrometer (4, 8), we chose a contact radius R = 0.5 μm. The length scale here is simply $r = 2R = 1$ μm (i.e., the approximate length of a typical FA).

In this case, the relaxed stiffness can be calculated as $k(t) \approx G(t) \cdot r$, with the relaxation test data shown in Figs. 4*B* and 5*B* for both kinds of ECMs. Once the relaxed stiffness curve is obtained, the regularized Inverse Laplace Transformation (9) was employed to extract the relaxation time spectrum (Figs. 4*C* and 5*C* and Fig. S6*B*), where each peak corresponds to a distinct relaxation timescale exhibited by the viscoelastic material. To test whether the fitting formula

$$S(t) = 1 - \sum_i H(\tau_i) e^{-\frac{t}{\tau_i}}, \qquad \textbf{[S10]}$$

by including the distinct peaks, τ_i, identified from the relaxation spectrum, can indeed match the measured relaxed stiffness, their comparisons are given in Figs. 4B, *Inset* and 5*B*, *Inset*. Note that here we normalized the relaxed stiffness $S(t)$ by the initial stiffness $k_a + k_l$, and the peak height $H(\tau_i)$ indicates the relaxed weight percentage for timescale τ_i. Clearly, excellent fitting has been achieved. Next, we need to select an effective timescale from the spectrum. From our timescale analysis (Fig. 3), only relaxation timescales that are larger than the characteristic binding time (i.e., $\tau_s \geq \tau_b$) will play a significant role in the viscosity regulation. Thus, the highest peak larger than binding timescale ($\tau_s \geq \tau_b$) is chosen as the effective timescale. The effective additional stiffness $(k_a + k_l)H(\tau_{s,eff})$ and viscosity $\tau_{s,eff}(k_a + k_l)H(\tau_{s,eff})$ can also be calculated. In addition, all small peaks (with amplitude less than 0.05) in the spectrum were ignored in our analysis.

To fit the experimental data reported by Chaudhuri (5), a scaling factor SF = 0.3 was introduced [i.e., assuming $k(t) \approx SF \cdot G(t) \cdot r$] to account for possible variations in the clutch and myosin numbers among different cell types. The fitting from time spectrum analysis is shown in Fig. S6. Besides, note that the 4-h cell spreading data (Fig. 4*D*) are used for substrates made of cross-linked polyacrylamide (elastic) and linear polyacrylamide (viscous), indicating that viscosity increases cell spreading. However, experiments on cell projected area for a longer time (24 h) shows similar spreading area on both elastic and viscoelastic gels (10). We believe that this evolution of cell spreading can be attributed to chemical or biological feedbacks at longer timescales, such as the weakening of clutch reinforcement, which is not included in our model.

Simulation with Multiple Relaxation Timescales

To incorporate multiple relaxation timescales into our model, we replaced the standard linear viscoelastic model with the generalized Maxwell model. In this model, one spring (with long-term stiffness k_l) and multiple Maxwell elements (with additional stiffness $k_{a,i}$ and viscosity η_i) are assembled in parallel. The constitutive equations (Eq. **S4**) can be rewritten as

$$\sigma_i = \eta_i \frac{dx_{\eta,i}}{dt} = k_{a,i}\left(x_s - x_{\eta,i}\right),\ i = 1,2,\ldots,n \qquad \textbf{[S11]}$$

$$k_l x_s + \sum_{i=1}^{n} \sigma_i = F_s. \qquad \textbf{[S12]}$$

Here k_l and $k_{a,i}$ are the long-term stiffness and *i*th additional stiffness, respectively, and η_i, $x_{\eta i}$, and σ_i represent the viscosity,

displacement, and force, respectively, for i th dashpot (Fig. S8*A*). In this way, the model possesses n relaxation timescales (i.e., $\tau_{s,i} = \eta_i / k_{a,i}$) and yields n ordinary deferential equations (ODEs). The motor clutch framework described by other equations (Eqs. **S1**–**S3** and **S5**) remains valid in this case. Together, there are $n + 2$ ODEs, which can be solved by the ODE solver (ode15s) in MATLAB.

We find that, by using the generalized Maxwell model, the cell spreading speed increases by only 4% (from 97.2 nm/s to 101.1 nm/s) for substrates synthesized by combining cross-linked polyacrylamide with linear acrylamide (Fig. S8*B*), while the speed remains almost the same (increase from 74.6 nm/s to 75.4 nm/s) for substrates with covalent cross-linkers and supramolecular cross-linkers (Fig. S8*C*). Similar results are also obtained for alginate substrates (5). Furthermore, we also examined the influence of a second relaxation timescale on spreading speed. Specifically, we chose the first timescale to be $\tau_{s,1} = 1$ s and swept the second timescale $\tau_{s,2} = \eta_2 / k_{a,2}$ over a broad range. The simulation results verify our main conclusion that the timescales larger than binding timescale (i.e., $\tau_s > \tau_b$ in the gray region) play more significant roles in cell spreading compared with other timescales (Fig. S8*D*).

General Model Parameters

Except for the steady spreading timescale, relaxation timescales, and stiffness values, which are measured from experiments (see *Initial Spreading Speed Determines the Final Spreading Area*), all of the other parameters are kept constant for all simulations. The values of each parameter are listed in Table S1, with their references. Some of the values deserve additional elaboration.

The value of the characteristic breakage force F_b was chosen as 1.3 pN for the analytical solution generalized by mean-field theory, which is slightly smaller than the value of 2 pN used in the KMC simulations. This is because we directly used the average clutch force F_c in the exponential expression of r_{off} to calculate its mean. The reduction in the characteristic breakage force simply accounts for the average bias of the nonlinear exponential term.

The value of the threshold average clutch force (3 pN) characterizes the collective critical force for FA reinforcement, which determines the rigidity (~1 pN/nm) at which the integrin density (hence binding rate) begins to increase. Here we chose the average force over the lifetime as the threshold rather than the maximum force on a single clutch. The reason is that the analytical solution is derived from mean-field theory, which represents the ensemble behavior of all clutches. Consequently, the value is smaller than the previous reported threshold clutch force value (4, 11), because the maximum clutch force is diluted in the average. Generally, the simulated maximum force is around 30 pN, one order of magnitude larger than the average value, which agrees with the experimental measurements (11).

The characteristic length for the FAs was set at 1 μm, which is adapted from a previous study (4). The size of the FAs will not significantly change the model predictions, since the clutch number is fixed (6, 12). Different FA sizes only change the characteristic length scale for the unit conversion from kilopascal to piconewton per nanometer. However, considering that FAs are elongated and elliptical, the area of an elongated FA with a larger length should be comparable to the area of a circle with the length of 1 μm. Thus, 1 μm is a reasonable estimate for the characteristic length of an FA.

The value of parameter α characterizes the sensitivity of the binding rate with increased clutch force. Physically, it determines how fast the binding rate would increase with stiffness. To determine the value for this parameter, we fit our simulation for the purely elastic substrate across different stiffness levels. As seen in Fig. S7, the value of 0.2/pN leads to an excellent fit for the experimental data. Note that parameter α is not very sensitive for the model, as a larger α only leads to a sharp increase of speed at a stiffness of ~1 pN/nm.

1. Nisenholz N, Paknikar A, Köster S, Zemel A (2016) Contribution of myosin II activity to cell spreading dynamics. *Soft Matter* 12:500–507.
2. Nisenholz N, et al. (2014) Active mechanics and dynamics of cell spreading on elastic substrates. *Soft Matter* 10:7234–7246.
3. Bangasser BL, Odde DJ (2013) Master equation-based analysis of a motor-clutch model for cell traction force. *Cell Mol Bioeng* 6:449–459.
4. Elosegui-Artola A, et al. (2014) Rigidity sensing and adaptation through regulation of integrin types. *Nat Mater* 13:631–637.
5. Chaudhuri O, et al. (2015) Substrate stress relaxation regulates cell spreading. *Nat Commun* 6:6364.
6. Chan CE, Odde DJ (2008) Traction dynamics of filopodia on compliant substrates. *Science* 322:1687–1691.
7. Walcott S, Sun SX (2010) A mechanical model of actin stress fiber formation and substrate elasticity sensing in adherent cells. *Proc Natl Acad Sci USA* 107:7757–7762.
8. Plotnikov SV, Pasapera AM, Sabass B, Waterman CM (2012) Force fluctuations within focal adhesions mediate ECM-rigidity sensing to guide directed cell migration. *Cell* 151:1513–1527.
9. Provencher SW (1982) CONTIN: A general purpose constrained regularization program for inverting noisy linear algebraic and integral equations. *Comput Phys Commun* 27:229–242.
10. Charrier EE, Pogoda K, Wells RG, Janmey PA (2018) Control of cell morphology and differentiation by substrates with independently tunable elasticity and viscous dissipation. *Nat Commun* 9:449.
11. Roca-Cusachs P, Iskratsch T, Sheetz MP (2012) Finding the weakest link: Exploring integrin-mediated mechanical molecular pathways. *J Cell Sci* 125: 3025–3038.
12. Bangasser BL, et al. (2017) Shifting the optimal stiffness for cell migration. *Nat Commun* 8:15313.

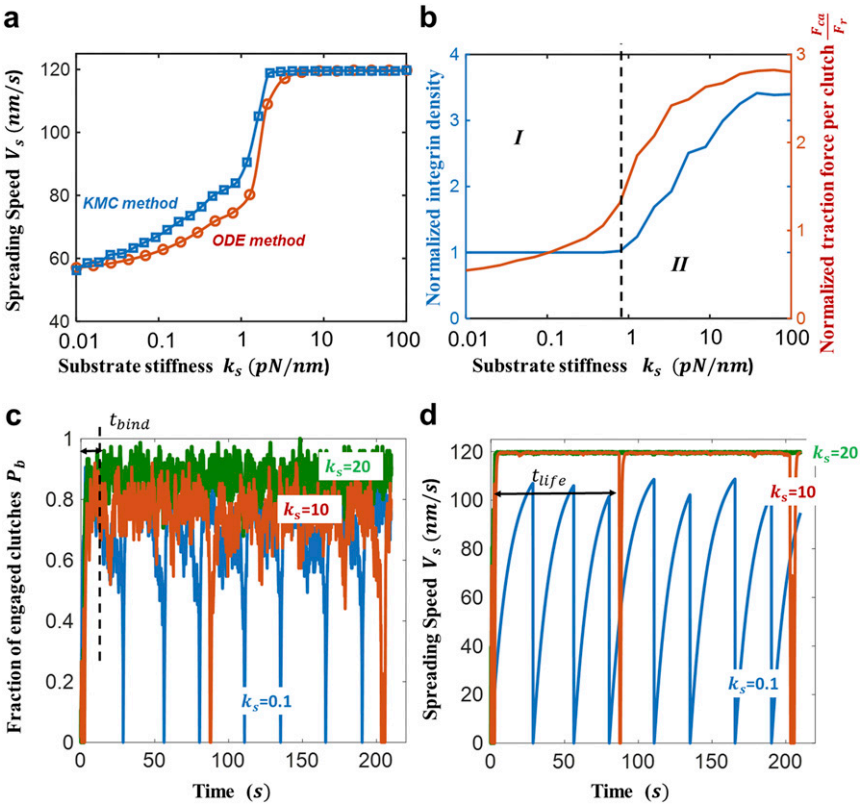

Fig. S1. (*A*) The mean spreading speed, V_s, as a function of substrate stiffness, k_s, calculated from the KMC (blue line) and the ODE method (red line). (*B*) Variations of the normalized integrin density (blue line) and traction force per clutch, F_{ca}/F_r, (red line) with respect to the substrate stiffness. Here the clutch reinforcement takes place when substrate stiffness is over 1 pN/nm (regime II). The dashed line indicates the critical stiffness where the reinforcement takes effect. Evolutions of the (*C*) fraction probability and (*D*) spreading speed for different stiffness values, i.e., $k_s = 0.1$ pN/nm (blue line), $k_s = 10$ pN/nm (red line), and $k_s = 20$ pN/nm (green line), obtained from KMC simulations. The binding time t_{bind} and lifetime t_{life} are marked for $k_s = 10$ pN/nm. It is clear that the clutch reinforcement for $k_s = 10$ pN/nm and 20 pN/nm significantly increases the spreading speed and FA lifetime. The FA becomes much stable for $k_s = 20$ pN/nm as a high percentage of clutches remain engaged.

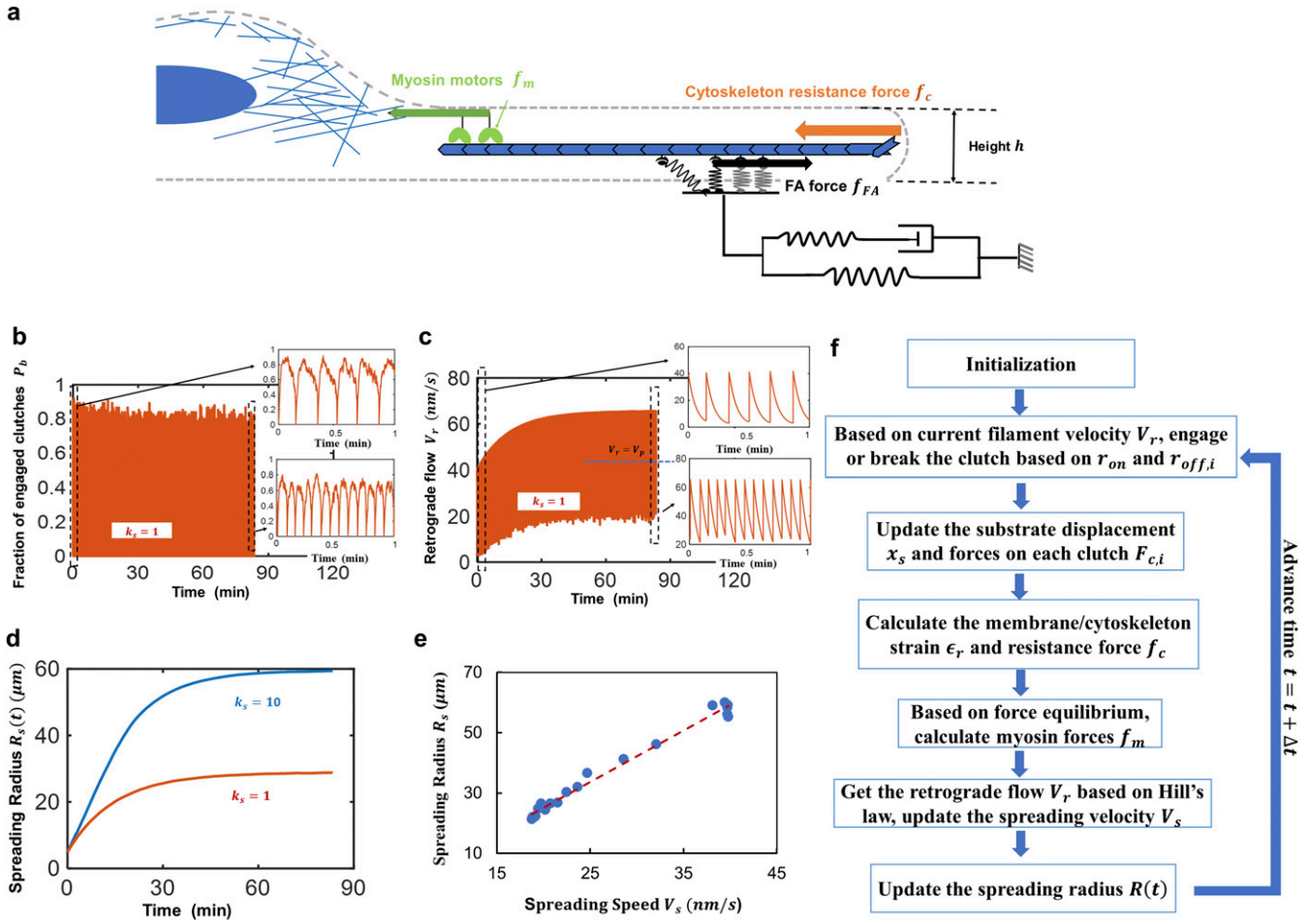

Fig. S2. (*A*) Schematic of the cell spreading model based on the motor clutch framework. The forces shown in *A*, i.e., myosin motor force f_m, cytoskeleton resistance force f_c, and FA force f_{FA}, are involved during spreading. (*B*) The fraction of engaged clutches, P_b, and (*C*) the retrograde flow, V_r, predicted from the KMC method for $k_s = 1$ pN/nm (red line) and $k_s = 10$ pN/nm (blue line). (*Insets*) The two enlarged plots in *B* and *C* illustrate how the P_b and V_r evolve in the first and the last 1 min for $k_s = 1$ pN/nm, which indicates a constant load and fail behavior of the FA. (*D*) The spreading radius, $R_s(t)$, plotted as a function of time for $k_s = 1$ pN/nm (red line) and $k_s = 10$ pN/nm (blue line). (*E*) The steady-state spreading radius plotted as a function of the initial spreading speed V_s. Here the substrate stiffness k_s was varied in the simulations to achieve different initial spreading speeds (and hence different steady-state spreading radius), while other parameters were chosen to be $R_0 = 5$ μm, $k_m = 0.1$ pN/nm, $\eta_m = 1$ pN·s/nm, $h = 0.2$ μm, and $V_p = 40$ nm/s. The blue circles are the simulation results, and the dashed line indicates a linear relation between V^s and R^s. (*F*) The flowchart depicting the simulation algorithm for getting the steady-state spreading configuration.

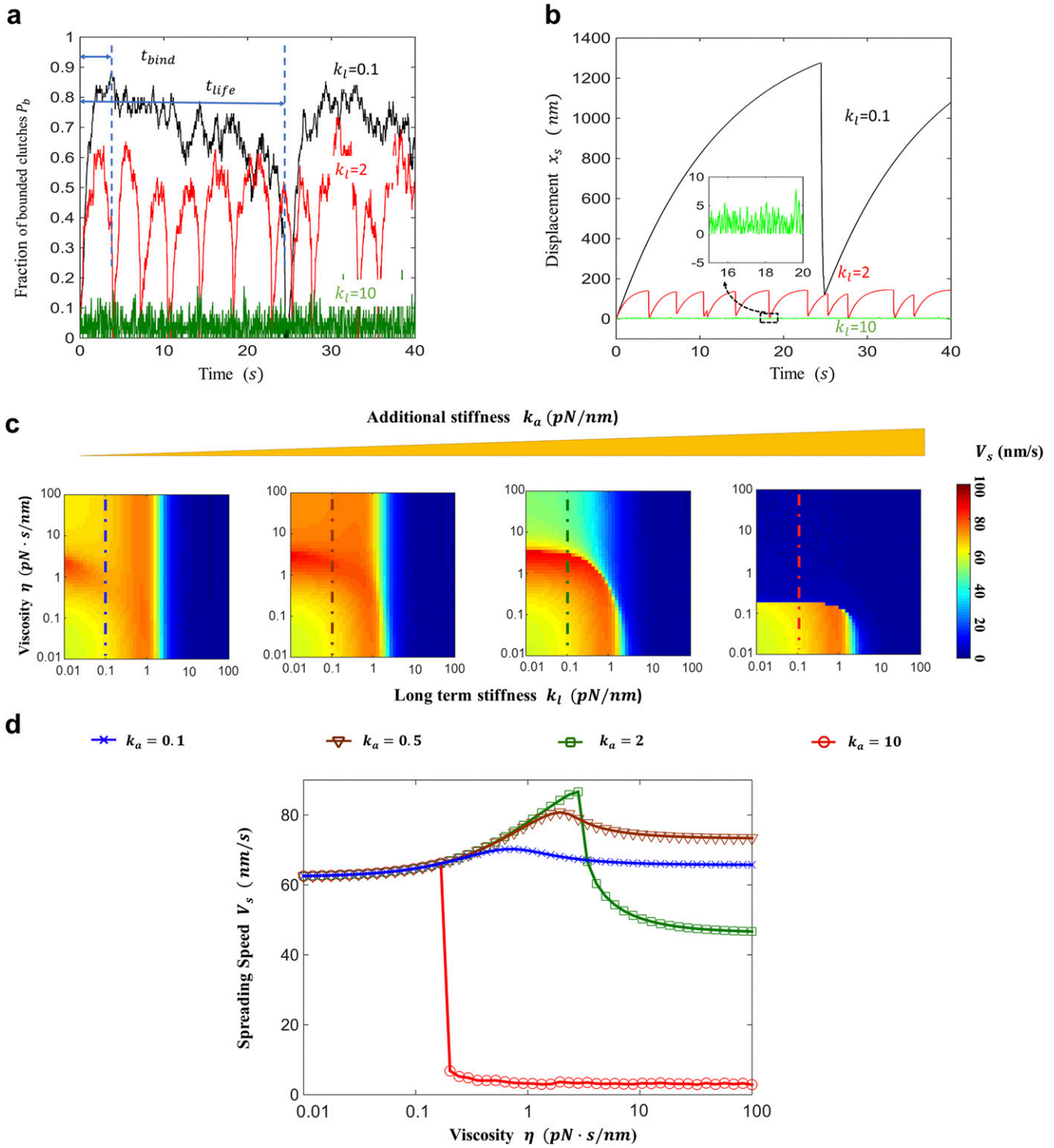

Fig. S3. Cell spreading speed is significantly different based on the elastic and viscous parameters (k_a, k_l, η) of the substrate without any clutch reinforcement. (*A* and *B*) The KMC method produced (*A*) the fraction probability and (*B*) the substrate displacements for three typical values of k_l, showing that the stable binding time t_{bind} and lifetime t_{life} influence FA behavior. A fixed stiffness k_a = 1 pN/nm was chosen for all plots. (*Inset*) An enlarged plot of substrate displacement for k_l = 10 pN/nm exhibiting frictional slippage behavior. (*C*) Heat maps of spreading speed, V_s, are plotted as a function of long-term stiffness, k_l, and viscosity, η, from the ODE method. The substrate additional stiffness, k_a, increases from 0.1 pN/nm to 10 pN/nm from *Left* to *Right*. (*D*) Mean spreading speed versus viscosity, η, for four different values of k_a corresponding to the dashed lines in *C* with k_l = 0.1 pN/nm. There is an optimum viscosity that maximizes cell spreading, which becomes more significant as k_a increases from 0.1 pN/nm to 2 pN/nm. Above k_a = 5 pN/nm, the substrate behaves like a Kelvin–Voigt model with a sharp decrease in cell spreading with viscosity.

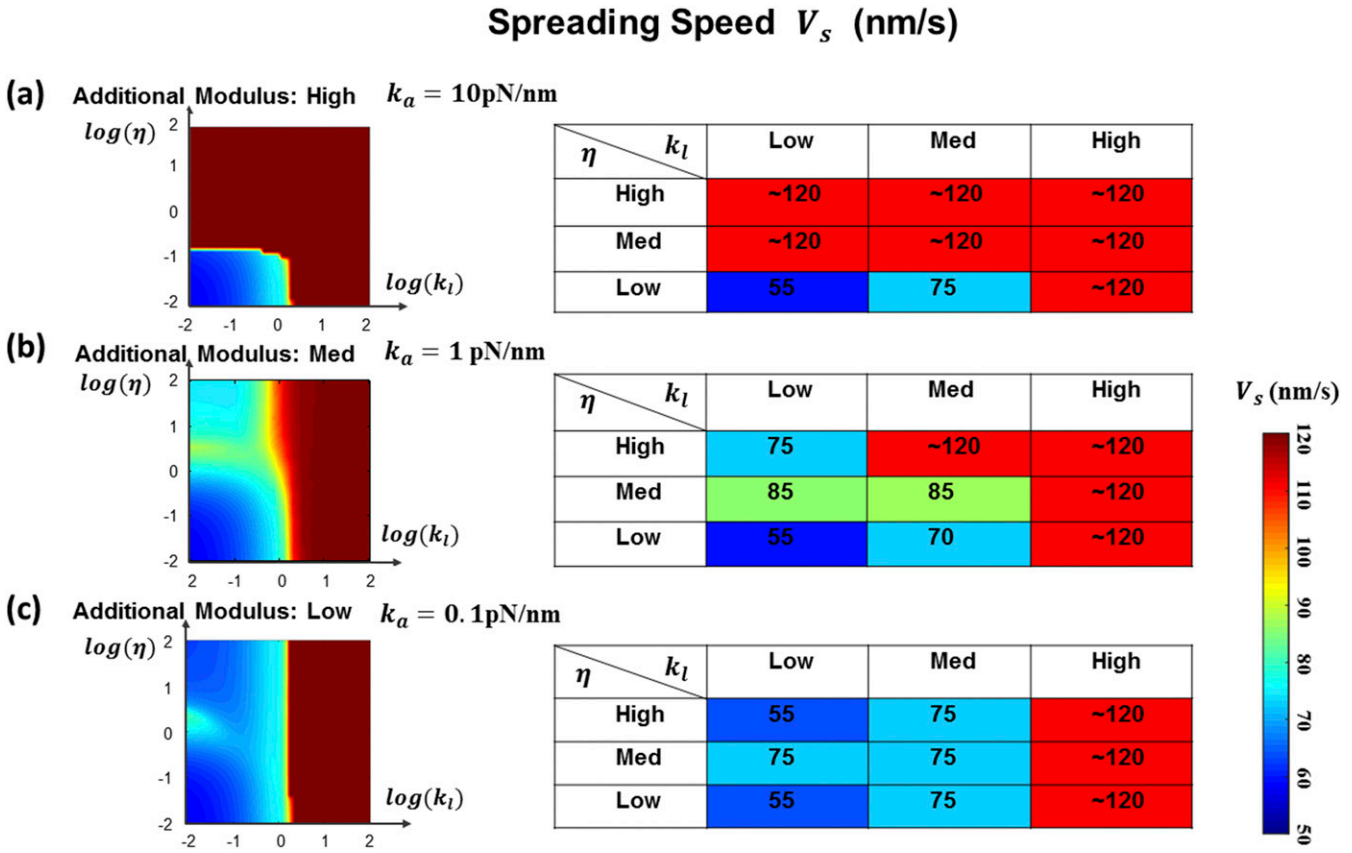

Fig. S4. (*A–C*) Heat maps and corresponding tables of the mean spreading speed, V_s, shown as a function of the long-time stiffness, k_l, viscosity, η, and additional stiffness,k_a, in three different levels: low, medium, and high for each parameter. *A–C* represent high, medium, and low levels of additional modulus, k_a, respectively. The values in tables show the representative spreading speed in each level of parameter. Different viscoelastic parameters lead to distinct regulation effects on cell spreading.

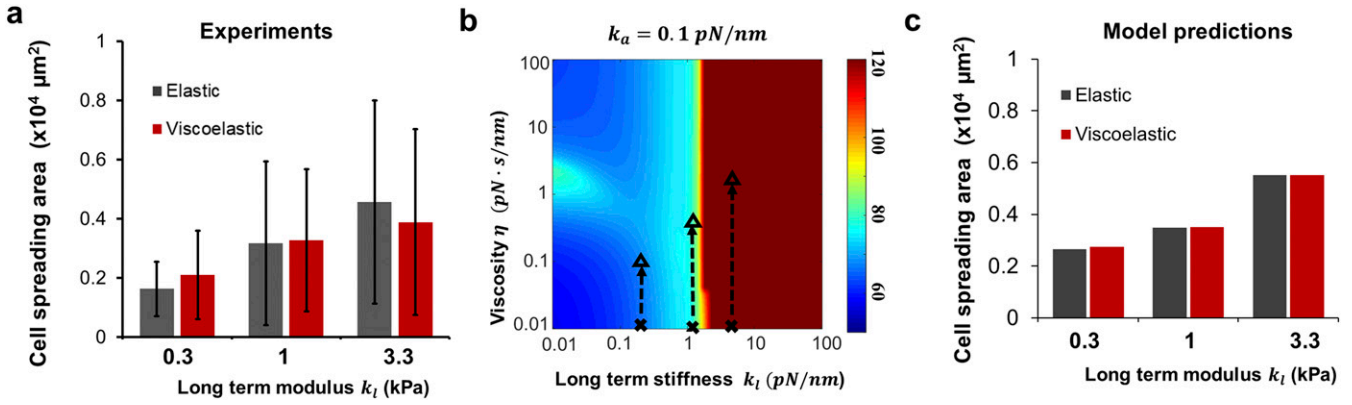

Fig. S5. (*A*) Cell spreading area measured on covalent cross-linking ECM (elastic, gray column) and covalent and supramolecular cross-linking ECM (viscoelastic, red column). Cell spreading area was similar for elastic and viscoelastic substrates for three different stiffness cases (no significant difference is observed based on Student's tests). (*B*) Heat map of spreading speed, V_s, plotted as a function of long-term stiffness, k_l, and viscosity, η, for small additional stiffness, k_a = 0.1 pN/nm. Black markers indicate the mechanical parameters of the elastic (cross markers) and viscoelastic (triangle markers) substrates based on the relaxation tests. (*C*) Model prediction of cell spreading area on elastic and viscoelastic substrates based on points indicted in *B*. Clearly, the simulation results fit the experimental data quite well. The data are shown with mean ± SD, with $n \geq 80$ cells for each measurement.

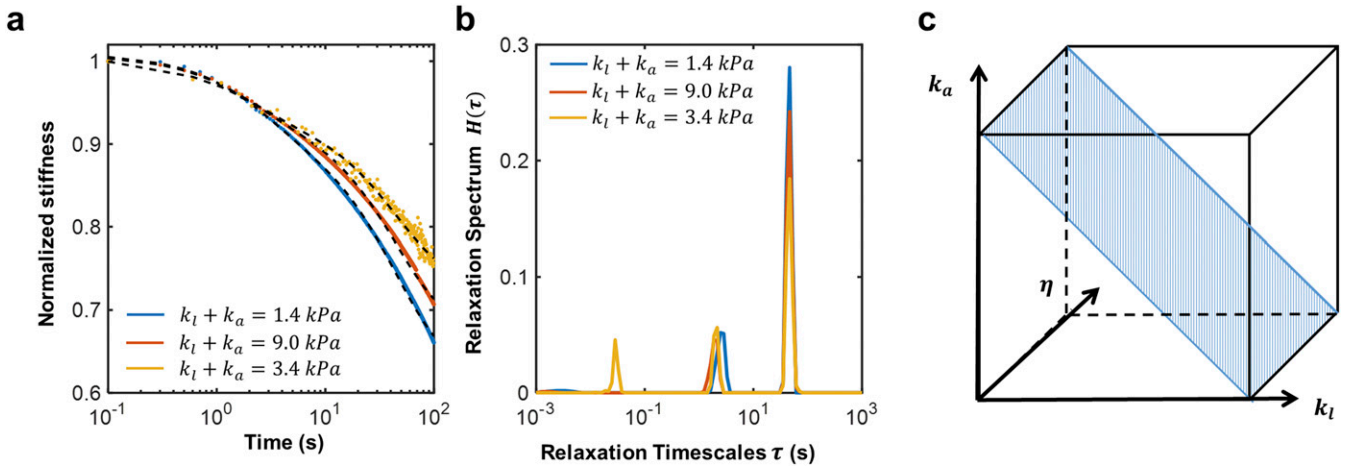

Fig. S6. (*A*) Measured normalized relaxed stiffness of alginate substrates (covalent and ionic) with different initial moduli. The black dashed lines correspond to the fitting results with characteristic relaxation timescales identified in *B*. (*B*) Relaxation spectra of different alginate substrates which indicate a common dominant relaxation timescale of $\tau_s = 15$ s. (*C*) Schematic plot of the plane corresponding to a fixed initial stiffness in the space spanned by three viscoelasticity parameters. Results shown in Fig. 6 *A*–*C* were based on simulations with parameters selected from this plane.

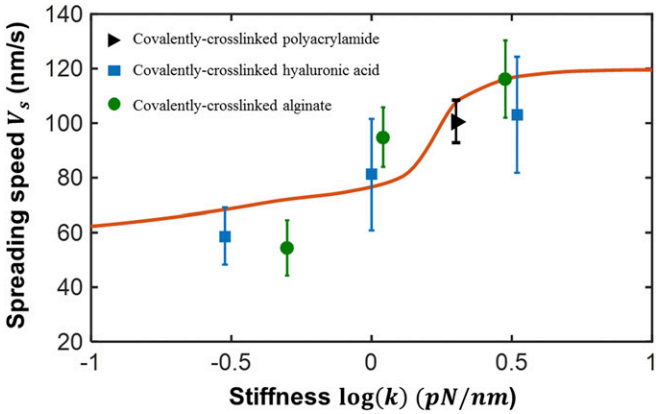

Fig. S7. The predicted spreading speed (red line) plotted as a function of stiffness with the reinforcement mechanism. The experimental data for different purely elastic substrates are shown with error bars. Black triangle, covalently cross-linked polyacrylamide elastic substrate corresponding to Fig. 4; blue square, covalently cross-linked hyaluronic elastic substrate corresponding to Fig. 5 and Fig. S5; green circle, covalently cross-linked alginate elastic substrate corresponding to Fig. 6. The spreading speed is extracted from measured spreading area by assuming fixed initial radius and steady timescale for the corresponding cell type (*Initial Spreading Speed Determines the Final Spreading Area* and *General Model Parameters*).

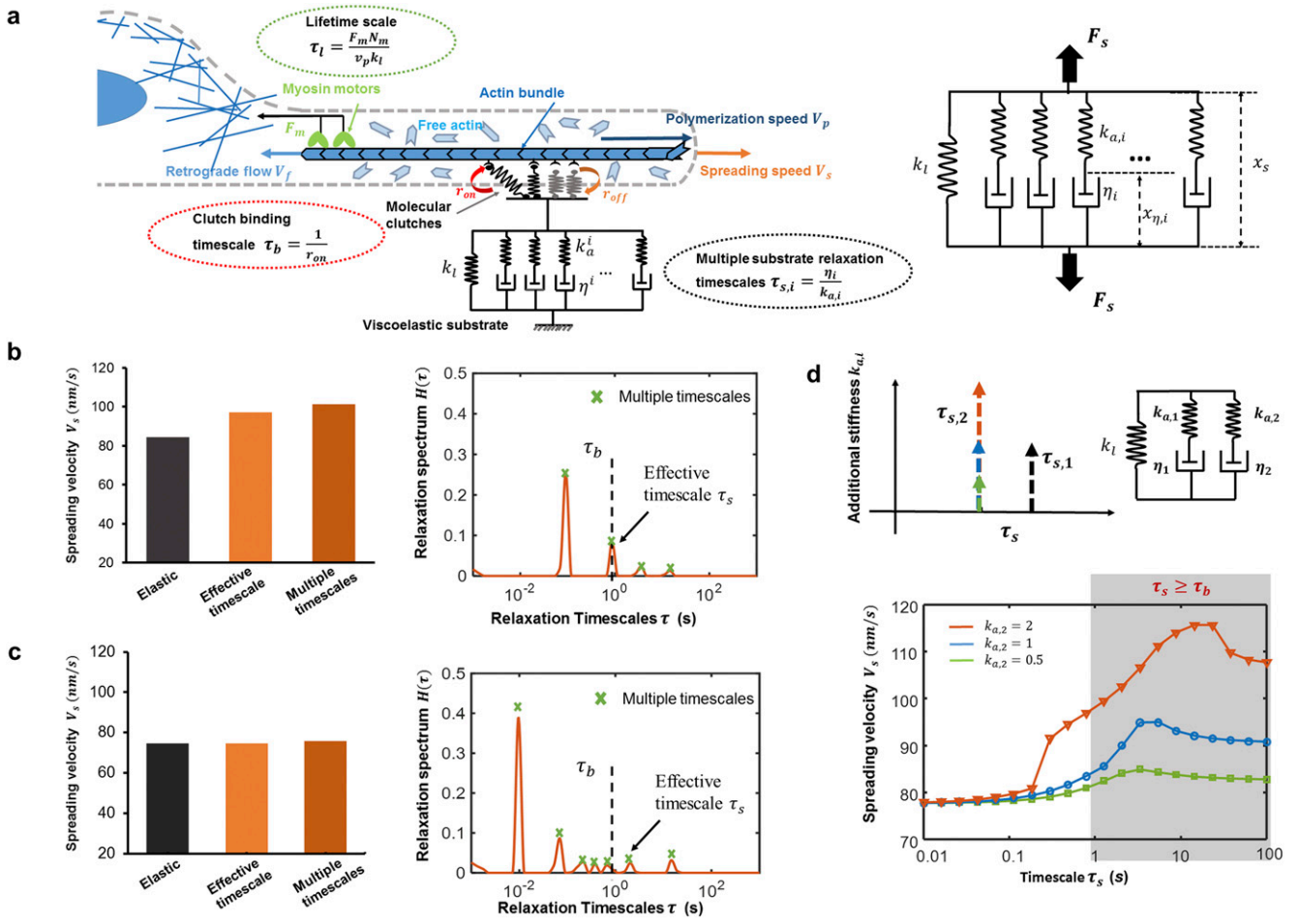

Fig. S8. (*A*) Schematic of the motor-clutch model incorporated with a viscoelastic substrate that has multiple relaxation timescales (generalized Maxwell model). In this generalized Maxwell model, one spring (with long-term stiffness k_l) and multiple Maxwell elements (with additional stiffness $k_{a,i}$ and viscosity η_i) are assembled in parallel. (*B* and *C*) Simulations using multiple relaxation timescales give results (*Left*) close to the case of a single effective timescale: (*B*) results for substrates of cross-linked polyacrylamide mixed with linear acrylamide corresponding to Fig. 4, and (*C*) results for substrates composed of covalent and supramolecular cross-linkers corresponding to Fig. 5. (*Right*) The chosen multiple timescales are shown with crosses (x) in the relaxation spectra. (*D*) The cell spreading speed, V_s, plotted as a function of substrate second timescale $\tau_{s,2}$ for different second additional stiffness values ($k_{a,2} = 0.5$, 1, and 2 pN/nm). Here we set $k_{a,1} = 1$ pN/nm, $\eta_1 = 1$ pN·s/nm (i.e., $\tau_{s,1} = 1$ s), and $k_l = 0.1$ pN/nm. The simulation results indicate that the timescales larger than binding timescale (i.e., $\tau_s \geq \tau_b$) play a more significant role in cell spreading compared with other timescales.

Table S1. List of parameters in the model

Parameters	Meaning	Value	Source
n_m	Myosin motor number	75	(1, 2)
F_m	Myosin force	2 pN	(1, 2)
F_{cr}	Threshold Reinforcement force	3 pN	Adjusted based on refs. 3 and 4 (*General Model Parameters*)
n_c	Clutch number	75	(1, 2)
F_b	Characteristic breakage force	2 pN	(1, 2)
r_{on}^0	Binding rate	1 s^{-1}	(1, 2)
r_{off}^0	Zero force dissociation rate	0.1 s^{-1}	(1, 2)
k_c	Clutch stiffness	5 pN/nm	(1, 2)
v_u	Unloaded retrograde flow velocity	120 nm/s	(1, 2)
V_p	Polymerization speed	120 nm/s	(1, 2)
k_s	ECM stiffness (k_l, k_a)	10^{-2} pN/nm to 10^2 pN/nm	This article
η	Viscosity	10^{-2} pN·s/nm to 10^2 pN·s/nm	This article
α	Integrin density increment rate	0.2 per piconewton	Fitting parameters (*General Model Parameters*)
h	Thickness of lamellipodium	200 nm	Adjusted based on refs. 5 and 6
R_0	Initial spreading radius	5 μm	Adjusted based on ref. 6
τ_{ss}	Timescale for steady spreading	100 s to 400 s	Adjusted based on refs. 5 and 6
r	Characteristic length	∼1 μm	Adjusted based on refs. 3 and 4 (*Extracting Substrate Parameters from Relaxation* Test and *General Model Parameters*)

1. Bangasser BL, Odde DJ (2013) Master equation-based analysis of a motor-clutch model for cell traction force. *Cell Mol Bioeng* 6:449–459.
2. Chan CE, Odde DJ (2008) Traction dynamics of filopodia on compliant substrates. *Science* 322:1687–1691.
3. Elosegui-Artola A, et al. (2014) Rigidity sensing and adaptation through regulation of integrin types. *Nat Mater* 13:631–637.
4. Elosegui-Artola A, et al. (2016) Mechanical regulation of a molecular clutch defines force transmission and transduction in response to matrix rigidity. *Nat Cell Biol* 18:540–548.
5. Nisenholz N, Paknikar A, Kster S, Zemel A (2015) Contribution of myosin II activity to cell spreading dynamics. *Soft Matter* 12:500–507.
6. Nisenholz N, et al. (2014) Active mechanics and dynamics of cell spreading on elastic substrates. *Soft Matter* 10:7234–7246.